Available online at www.sciencedirect.com
ScienceDirect
Journal of Catalysis 253 (2008) 139–147
JOURNAL OF CATALYSIS
www.elsevier.com/locate/jcat

Kinetics and mechanism of NO reduction with CO on Ir surfaces

T. Fujitani *, I. Nakamura, A. Takahashi, M. Haneda, H. Hamada

Research Institute for Innovation in Sustainable Chemistry, National Institute of Advanced Industrial Science and Technology (AIST), 16-1 Onogawa, Tsukuba, Ibaraki 305-8569, Japan

Received 4 September 2007; revised 10 October 2007; accepted 12 October 2007

Available online 19 November 2007

Abstract

The adsorption and thermal reactivity of NO and CO and the kinetics of the NO reduction with CO on Ir surfaces were studied using X-ray photoelectron spectroscopy, polarization modulation infrared reflection–absorption spectroscopy, and temperature programmed desorption. The NO adsorption and dissociation activity was strongly dependent on the Ir surface structure. The NO dissociation activity of the Ir planes decreased in the order (100) > (211) ≫ (111). In contrast, the type of the CO adsorption site was independent of the Ir surface structure. The activity of Ir(111) for N_2 and CO_2 production from the NO + CO reaction was low compared with the activities of Ir(100) and Ir(211). The kinetic data for an Ir/SiO_2 powder catalyst were similar to data obtained for Ir(211). The order of the turnover frequencies for N_2 and CO_2 formation for the Ir planes was in good agreement with the order for NO dissociation activity, and this agreement indicates that the catalytic activity for NO reduction was dependent on NO dissociation. A kinetic study of the elementary steps indicated that the rate-limiting step for NO reduction with CO was the NO dissociation step.

Keywords: Ir single crystal; Ir/SiO_2; X-ray photoelectron spectroscopy; Polarization modulation infrared reflection–absorption spectroscopy

1. Introduction

Selective catalytic reduction is a promising method for removing NO, a pollutant emitted from diesel engines, lean-burn engines, and combustors. Numerous studies have investigated the selective catalytic reduction of NO using reductants such as NH_3 and hydrocarbons [1–3]. H_2 and CO have not been regarded as effective reductants in the presence of O_2, because they are more easily oxidized by O_2 than by NO. Recently, Ir-based catalysts were found to be effective for the selective reduction of NO with CO in the presence of O_2. Ogura et al. [4] found that NO is selectively reduced with CO on Ir/silicalite in an oxidizing atmosphere. Wang et al. [5] investigated the reduction of NO with CO over Pd/ZSM-5, Pt/ZSM-5, Ir/ZSM-5, and Rh/ZSM-5 catalysts in the presence of excess oxygen; of these catalysts, Ir/ZSM-5 exhibits the highest activity. Ir/SiO_2 has also been reported to be an excellent catalyst for the reduction of NO by CO in the presence of O_2 and SO_2 [6]. Shimokawabe and Umeda [7] examined the reduction of NO by CO in the presence of excess O_2 and found that of seven metals (Ag, Cu, Fe, Ir, Pd, Pt, and Rh) supported on metal oxides, Ir/WO_3, Ir/ZnO, and Rh/Al_2O_3 show the most pronounced catalytic activities for the reduction of NO by CO. Takahashi et al. [8] also reported that the catalytic activity for the selective reduction of NO with CO over Ir/SiO_2 is greatly increased by the addition of a W species.

The reaction of NO and CO has been studied over various transition- and noble-metal catalysts because of its importance for three-way catalytic converters [9–13]. However, clarifying the reaction mechanism, kinetics, and the role of the active site using only industrially applied heterogeneous catalysts is difficult. Single crystals and model catalysts provide well-defined surface geometries and allow detailed atomic-level characterization of the post-reaction surface and adsorbate-converted surface to be performed. These types of studies have clarified the dependence of the catalytic behavior on the crystal structure, in addition to providing information regarding the identity and role of the active site, reaction intermediates, promoters, and inhibiters [14,15]. Hopstaken et al. [16] and Root et al. [17] reported that the dissociation and desorption of NO from Rh(111)

* Corresponding author. Fax: +81 298 61 8172.
E-mail address: t-fujitani@aist.go.jp (T. Fujitani).

0021-9517/$ – see front matter
doi:10.1016/j.jcat.2007.10.011

are not markedly influenced by the presence of CO, whereas repulsion between NO and CO destabilizes CO. Lintz et al. [18,19] studied the elementary step for the NO + CO reaction using Pt, Pd, and Rh. In addition, the NO + CO reaction on model surfaces under high pressure has been studied, and these studies provide information on real reaction kinetics and in situ adsorption behavior. Goodman et al. [20,21] carried out a high-pressure kinetic study of the CO + NO reaction on Pd single crystals, model planar catalysts, and conventional high-surface-area Pd/Al_2O_3 catalysts. The study showed that the reaction rate is enhanced over the Pd(111) surface and over larger particles in the model supported catalysts relative to the rates over Pd(100), Pd(110), and smaller supported particles; these results indicate that an inactive atomic N species plays a role in determining the reaction rate. Schmieg et al. [22] studied the NO + CO reaction at high-pressure over Rh(111) and Rh(110) to investigate the effect of the Rh surface structure and selectivity; they showed the NO + CO reaction is sensitive to the Rh structure primarily with regard to the selectivity of the reaction for N_2O production. However, the reaction mechanism, kinetics, and adsorption behavior for the NO + CO reaction on Ir-based catalyst surfaces are not fully understood [23,24].

In this study, we investigated the adsorption and thermal reactivity of NO and CO over Ir single crystals to clarify the influence of the Ir surface structure. Furthermore, we examined the kinetics and mechanism of the NO + CO reaction over Ir single crystals at high-pressure and compared the results with results for a conventional Ir/SiO_2 powder catalyst.

2. Experimental

2.1. Apparatus

X-ray photoelectron spectroscopy (XPS) experiments were performed in an ultrahigh-vacuum (UHV) apparatus composed of two chambers (VG, ESCALAB 220-i): a surface-analysis chamber ($<1 \times 10^{-10}$ Torr) and a preparation chamber ($<1 \times 10^{-8}$ Torr). The analysis chamber was equipped with an ion gun for Ar^+ sputtering, a photoelectron analyzer for XPS, and dosers for adjusting the NO and CO exposures. XPS spectra were measured with Mg$K\alpha$ radiation. Coverage was estimated by XPS on the basis of the oxygen-buildup curve at 300 K; the oxygen saturation coverage on the Ir surfaces was 0.5 (a coverage value (Θ) of 1 corresponds to the number of surface Ir atoms) [25]. The nitrogen, oxygen, and carbon coverages were determined from the N 1s/Ir $4f_{7/2}$, O 1s/Ir $4f_{7/2}$, and C 1s/Ir $4f_{7/2}$ peak area ratios, using the O 1s/Ir $4f_{7/2}$ peak area ratio obtained from the oxygen saturation coverage and the sensitivity factors for N 1s, O 1s, and C 1s [26].

The infrared reflection–absorption spectroscopy (IRAS, Mattson, RS/2) and temperature-programmed desorption (TPD) experiments were carried out in a UHV apparatus composed of four chambers: a load–lock chamber for changing samples ($<5 \times 10^{-10}$ Torr); a preparation chamber equipped with an ion gun for Ar^+ sputtering; an analysis chamber for the Auger electron spectroscopy (AES, OMICRON, SPECTALEED), and quadrupole mass spectroscopy (SPECTRA, VAC-CHECK) equipment ($<8 \times 10^{-11}$ Torr); and a reaction chamber in which the NO and CO adsorption experiments and reactions under high-pressure conditions (<1000 Torr) were performed. The pressure of the reaction chamber could be varied from 8×10^{-10} to 800 Torr. An IR spectrometer and the polarization modulation (PM) optics were situated in the reaction chamber (GWC Technologies, Model SSD-50; Hinds Instruments, Model PEM-50 Controller). The IR beam reflected from the surface was collected by a liquid-nitrogen-cooled mercury cadmium telluride IR detector. The photoelastic modulator controller was set to 2500 cm^{-1}. The PM-IRA spectra for the NO + CO reaction were recorded at a resolution of 4 cm^{-1} with 500 scans over a total measurement time of 5 min. The IRA spectra for the NO and CO adsorption experiments were recorded at a resolution of 4 cm^{-1} with 100 scans over a total measurement time of 30 s.

2.2. Kinetic measurements and testing of surface reaction properties

The NO + CO reaction to form CO_2 and N_2 was performed in a batch mode. The standard reaction gas pressures of NO (99.99%, TAIYO NIPPON SANSO Corporation) and CO (99.999% pure, TAIYO NIPPON SANSO Corporation) were 5 and 5 Torr, respectively. The NO was purified by five freeze–pump–thaw cycles using liquid nitrogen. The CO was in an Al cylinder and was trapped with a liquid nitrogen bath to exclude any metal carbonyls. The samples were controlled to the reaction temperature and the gate valve to reaction chamber and turbomolecular pump was closed, and then reactants were dosed in the reaction chamber. The reaction temperature was 573–723 K, and the reaction time was 60–90 min. After the reaction, He gas was fed through the reaction chamber at a total pressure of 760 Torr. The reaction gases diluted with He were analyzed with a micro gas chromatograph (μ-GC, Agilent, 3000A), which was directly connected to the reaction chamber. The μ-GC was equipped with a Molecular Sieve 5A column (for the analysis of N_2, NO, and CO) and a Porapak Q column (for the analysis of CO_2 and N_2O). Turnover frequencies (TOFs) were obtained by normalizing the gas-phase production per second to the total number of surface sites. The kinetic data for reaction on the Ir/SiO_2 catalyst were acquired in the flow mode with CO and NO partial pressures of 5 and 5 Torr, respectively, in a He carrier gas.

Adsorption experiments were carried out with ^{15}NO (99.9% pure, TAIYO NIPPON SANSO Corporation) and CO at 5×10^{-9} to 5×10^{-8} Torr (0–30 L; 1 L = 10^{-6} Torr s) and a sample temperature of 223 K. ^{15}NO gas was used to distinguish between N_2 and CO desorption peaks and between N_2O and CO_2 desorption peaks during TPD. The TPD experiments were performed with a 1.0 K/s heating rate.

2.3. Sample preparation

We used single-crystal discs of Ir(111), Ir(100), and Ir(211) (8-mm diameter, 1-mm thickness, 99.999% purity) polished on one side only. Ir(211) consists of three-atom-wide (111)

terraces separated by one-atom-high (100) steps. The crystal orientations were accurate to within 1°, and the surface roughnesses were <0.03 μm. The Ir surfaces were cleaned by cycles of Ar^+ sputtering and annealing in oxygen at 1000 K and then by annealing at 1250 K in a vacuum. The surface cleanliness of the samples was verified by XPS or AES.

Silica-supported Ir catalyst was prepared by impregnating SiO_2 (Fuji Silysia Chemicals, Cariact G-10, 300 m^2/g) with an aqueous solution of $H_2IrCl_6 \cdot 6H_2O$ (Soekawa Chemicals). The impregnated catalyst precursors were dried at 383 K and calcined at 873 K for 8 h in air. The loading of noble metals was fixed at 0.5 wt%. The number of exposed Ir atoms for Ir/SiO_2 was estimated by the amount of CO adsorption. The Ir dispersion was calculated to be 0.33% and the total number of active sites in the catalyst was estimated to be 2×10^{20} sites/g-Ir.

3. Results and discussion

3.1. NO reactivity on the Ir surfaces

We examined the NO adsorption behavior on the Ir(111), Ir(100), and Ir(211) surfaces using IRAS. Fig. 1 shows IRA spectra of the Ir surfaces exposed to NO at 223 K. We observed two peaks, at 1400–1444 and 1799–1820 cm^{-1}, during exposure of Ir(111) to 0.2–15 L of NO. The peak at 1799–1820 cm^{-1} was assigned to NO adsorbed on the atop site, and the peak at 1400–1444 cm^{-1} was due to NO adsorbed on the hollow site [23]. The intensity of the peak for atop NO increased with increasing NO exposure, and then saturated at 2 L. After the adsorption of atop NO was saturated, NO began to adsorb on the hollow site, and NO saturation coverage was obtained at

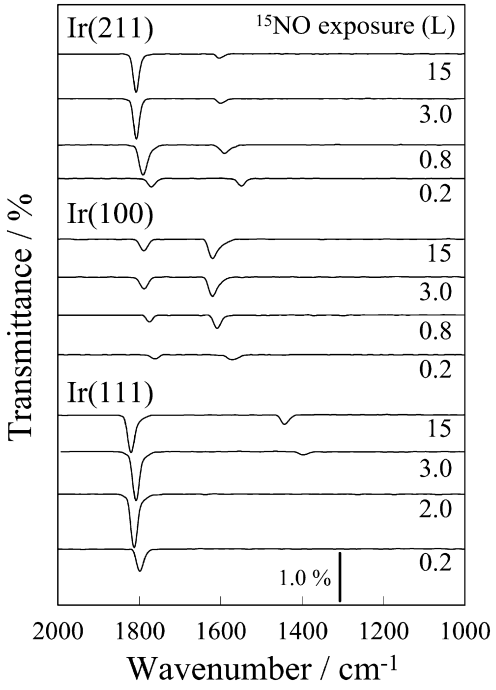

Fig. 1. IRA spectra of Ir(111), Ir(211), and Ir(100) after exposure to ^{15}NO at 223 K.

15 L. However, our previous XPS results indicated that the NO adsorption on hollow site was present even at low NO coverage [23]. Thus, it is possible that the NO simultaneously adsorbed on atop and hollow sites. From the O 1s peaks for XPS measurements, the saturation coverages of atop NO (532.8 eV) and hollow NO (530.4 eV) were estimated to be 0.15 and 0.32, respectively.

We observed two peaks, at 1570–1620 and 1760–1790 cm^{-1}, during exposure of Ir(100) to 0.2–15 L of NO. The peak at low frequency is in good agreement with peaks in the frequency region reported for NO adsorption on bridge sites of Rh(100) [27] and Pt(100) [28]. We therefore assigned the peak at 1570–1620 cm^{-1} to NO adsorbed on the bridge site of Ir(100). The peak at high frequency was observed at about 30 cm^{-1} lower than the peak observed for atop NO on Ir(111). Nyberg and Uvdal [29] reported that the frequency of atop NO on Pd(100) appears at 1667 cm^{-1}, which is about 30 cm^{-1} lower than for atop NO on Pd(111). We thus assigned the peak at 1760–1790 cm^{-1} to NO adsorbed on the atop site on Ir(100). The peak intensities of both atop NO and bridge NO increased with increasing NO exposure and saturated at about 3 L. We also investigated the NO adsorption process on Ir(100) using XPS and observed two O 1s peaks, at 531.2 and 532.8 eV, which were in good agreement with reported values for the binding energies of bridge NO and atop NO over Ni(100) [30] and Pt(111) [31], respectively. Saturation coverage was obtained at 3 L, where the saturation coverages of atop NO and bridge NO were 0.15 and 0.30, respectively.

On the Ir(211) surface, we observed two peaks, at 1547–1604 and 1768–1809 cm^{-1}, during exposure to 0.2–15 L of NO at 223 K. The peak at 1768–1809 cm^{-1} was assigned to NO adsorption on the atop site of the (111) terrace of Ir(211) [24]. The peak at 1547–1604 cm^{-1} was due to NO adsorbed on the bridge site of the (100) step over Ir(211) [24]. The coverage of both atop NO and bridge NO saturated at about 3 L. The saturation coverage of atop NO and bridge NO were 0.19 and 0.21, respectively, which were estimated from O 1s peaks at 531.2 and 532.8 eV.

We next examined the thermal reactivity of NO adsorbed on Ir(111), Ir(100), and Ir(211) (Fig. 2). In the TPD spectra for ^{15}NO and $^{15}N_2$ after saturation of the Ir(111) surface with ^{15}NO at 223 K, we did not observe any desorption peaks for $^{15}N_2O$ and O_2 up to 1300 K, which indicated that atomic oxygen (O_a) dissociated from NO diffused into the Ir subsurface. Two desorption peaks for ^{15}NO were observed, at 393 and 455 K, which were assigned to desorption of ^{15}NO adsorbed on the hollow and atop sites, respectively [23]. Simultaneously with ^{15}NO desorption, $^{15}N_2$ desorption peaks were observed at 471 and 574 K. We assigned these two $^{15}N_2$ peaks to a disproportionation reaction between atop NO and atomic nitrogen (N_a) dissociated from hollow NO and to the recombination of N_a, respectively [23]. A desorption peak for $^{15}N_2$ was observed at 390 K on Ir(100), whereas no desorption peak for ^{15}NO appeared. The adsorbed NO on the atop and bridge sites on Ir(100) completely dissociated to N_a at 350 K, as indicated by the XPS measurement. Therefore we assigned the desorption peak for $^{15}N_2$ at 390 K to the recombination of N_a from both adsorbed

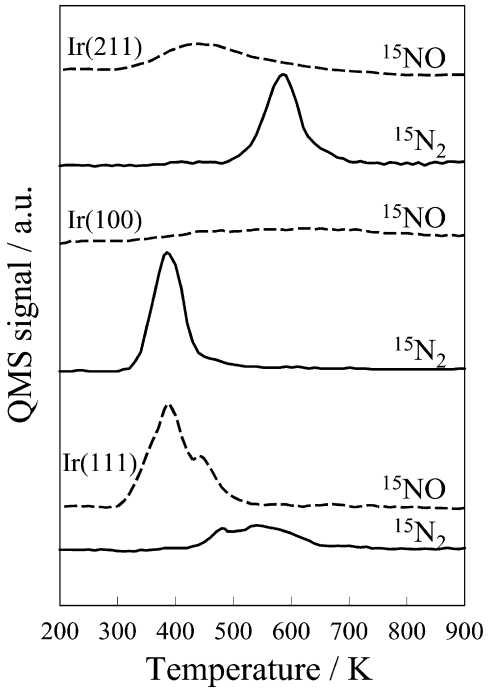

Fig. 2. TPD spectra for ^{15}NO adsorbed on Ir(111), Ir(211), and Ir(100).

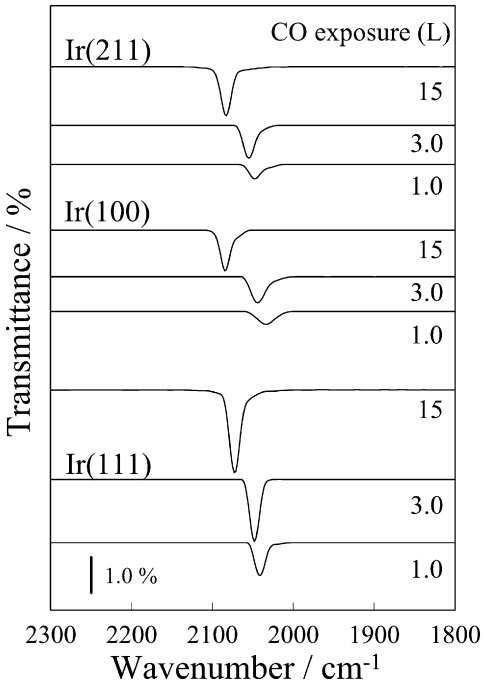

Fig. 3. IRA spectra of Ir(111), Ir(211), and Ir(100) after exposure to CO at 15 L and 223 K.

NO species on Ir(100). Furthermore, the desorption temperature for recombination of N_a on Ir(100) was 200 K lower than that on Ir(111), which indicates that the Ir(100) surface showed a high efficiency for N_2 formation from NO. In TPD spectra on Ir(211), the $^{15}N_2$ desorption peak was observed at 590 K, and a small ^{15}NO desorption peak was seen at 440 K, which indicates that almost all the ^{15}NO adsorbed on Ir(211) decomposed to $^{15}N_2$. We thus found that both atop NO and bridge NO dissociated on Ir(211). About twice as much N_2 formed on Ir(211) as on Ir(111), which indicates that the NO dissociation activity was higher over Ir(211) than over Ir(111).

The NO dissociation activity of the Ir planes decreased in the order (100) > (211) > (111). The thermal dissociation of NO is known not to occur on the low index planes such as Pd(111) and Pd(100) [32]. Stepped surfaces such as Pd(311) and Pd(112) are active for the thermal dissociation of NO [32,33]. In contrast, the (100) plane was the most active Ir surface structure for NO dissociation. However, the details of the dependence of the NO dissociation activity on surface structure were not clear.

3.2. CO reactivity on the Ir surfaces

We also investigated the adsorption properties of CO on Ir(111), Ir(100), and Ir(211). Fig. 3 shows the IRA spectra for the Ir surfaces at CO exposure of 1, 3, and 15 L at 223 K. The adsorbed CO peaks shifted to higher frequency with increasing CO exposure for all the Ir surfaces. The intensities and frequencies of adsorbed CO peaks on the Ir surfaces became constant above 10 L. For saturation CO coverage, a peak of CO adsorbed on atop sites was observed at 2073 cm^{-1} in the IRA spectra for the Ir(111) surface [23]. Peaks were observed at 2085 and 2083 cm^{-1} in the IRA spectra for Ir(100) and Ir(211), and these peaks were close to the peak for atop CO observed on the Ir(111) surface, which indicates that the CO was adsorbed on atop sites on Ir(100) and Ir(211).

We thus believe that CO adsorption site on the Ir surface was not dependent on the Ir surface structures. This result was very different from other transition metal surfaces such as Pd [34,35], Pt [36,37], and Rh [38,39]. It is very hard to discuss the difference in adsorption properties of Ir surface from only experimental results. We have been investigating the unique specificity of CO adsorption on the Ir surface using density functional theory (DFT) calculation.

On Ir(211), we could not determine whether the adsorption plane was the (111) terrace or the (100) step from the frequency of atop CO. The intensities of the atop-CO peak were dependent on the Ir surface structure. However, from the XPS results, we estimated that the saturated atop-CO coverage on all the Ir surfaces was 0.33, which suggests that the difference of the peak intensities for atop CO on the Ir surfaces was not due to adsorbed CO coverage. We also measured the initial adsorption rate for atop CO on the Ir surfaces from the build-up curve for CO adsorption using XPS (Fig. 4). From the slope of the line at zero coverage in Fig. 4, we estimated initial adsorption rate to be 7.3×10^{-4}–7.6×10^{-4} (molecules/(site s)) for all the Ir surfaces. Thus, we clearly show that the CO adsorption properties such as adsorption site, adsorption rate, and saturation coverage were not dependent on the Ir surface structure, which were different from the adsorption properties of other transition metal surfaces [34–39]. At present, the reason for the difference in adsorption properties of Ir surface is not clear.

We examined the thermal reaction properties of atop CO on the Ir surfaces. TPD spectra were obtained for the Ir surfaces after various CO exposures at 223 K (Fig. 5). CO desorption peaks at 550 and 640 K were observed for the Ir(111) and

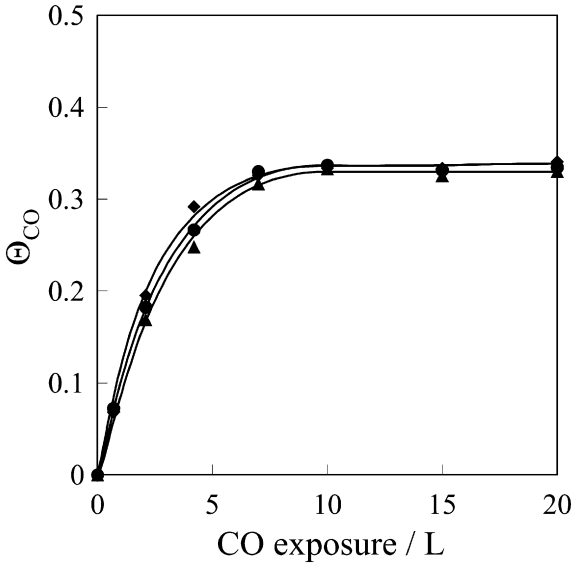

Fig. 4. Buildup of CO on Ir(111) (●), Ir(211) (▲), and Ir(100) (◆) at 223 K.

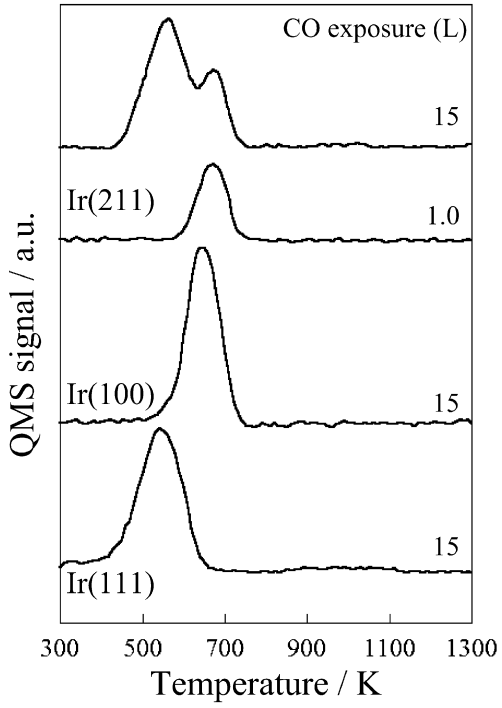

Fig. 5. TPD spectra for CO adsorbed on Ir(111), Ir(211), and Ir(100).

Ir(100) surfaces, respectively, exposed to 15 L of CO. Although the CO adsorption site was similar for both surfaces, the thermal stability of the CO adsorbed on Ir(100) was higher than that of the CO adsorbed on Ir(111). Orita calculated the adsorption energy of atop CO on Ir(111) and Ir(100) using DFT [40]. The CO adsorption energy on Ir(100) was 0.2–0.5 eV higher than that on Ir(111), which was in agreement with the thermal stability of the CO adsorbed on the Ir surfaces. A single CO desorption peak at 670 K was observed for the Ir(211) surface exposed to 1.0 L of CO; this temperature agrees with the desorption temperature of CO adsorbed on Ir(100), which indicates that the CO desorption peak at 670 K is due to atop CO on the (100) step over Ir(211). Above 2 L, a new desorption peak appeared at 560 K, and the area of the peak increased with increasing CO exposure up to 10 L. The temperature for this new desorption peak was close to the desorption temperature of CO adsorbed on Ir(111). We therefore identified the peak at 560 K as atop CO on the (111) terrace. We estimated the coverage for atop CO on the (111) terrace and (100) step over Ir(211) from the TPD peak area for the saturated CO-covered Ir(211) surface. The CO desorption ratios for the (111) terrace and the (100) step were about 2 and 1, respectively, and these values are in good agreement with the atomic ratios for the (111) terrace and (100) step over Ir(211). At low CO coverage, CO adsorbed only on the atop site of the (100) step. CO adsorption on the (100) step saturated at 2 L, and then CO began to adsorb at the (111) terrace above 2 L. We thus clarified the CO adsorption behavior by TPD experiments.

3.3. Reaction kinetics of NO reduction with CO on the Ir surfaces

The kinetics of the NO reduction with CO over the Ir single crystal and the powder Ir/SiO_2 catalyst were investigated under real reaction conditions. N_2 and CO_2 were formed by the reaction of NO + CO. No N_2O formation was observed on any of the Ir surfaces. The production ratios for N_2 and CO_2 were about 1 and 2, respectively, which indicates that the following reaction proceeded on the Ir metal surfaces:

$$NO + CO \rightarrow (1/2)N_2 + CO_2.$$

In addition to N_2 and CO_2, N_2O is produced from the NO + CO reaction ($P_{NO} = P_{CO} = 8$ Torr) over Rh(110) and Rh(111) [22]. Furthermore, high N_2O formation from the NO + CO reaction ($P_{NO} = P_{CO} = 1$ Torr) is observed on Pd single-crystal surfaces [20]. In particular, the N_2O selectivity on the Pd surface increases with increasing reaction temperatures. Thus, in comparison, the Ir metal surface has excellent selectivity for N_2 formation from the NO + CO reaction.

Fig. 6 shows Arrhenius plots of the TOFs for N_2 and CO_2 formation from the NO + CO reaction on the Ir surfaces as well as on an Ir/SiO_2 powder catalyst. As can be seen from the figure, the Ir(111) plane showed low activity for N_2 and CO_2 production compared with the Ir(100) and Ir(211) planes. The TOFs for N_2 and CO_2 formation for the Ir planes decreased in the order (100) $\geqslant$ (211) $\gg$ (111); for example, the TOF for N_2 formation at 600 K on Ir(100) was about 3 and 50 times the TOFs on Ir(211) and Ir(111), respectively. Table 1 summarizes the apparent activation energies and pre-exponential factors for N_2 and CO_2 formation over the Ir surfaces. The apparent activation energies for N_2 and CO_2 formation were estimated to be 107–115 and 110–120 kJ/mol, respectively; and these values were almost the same, regardless of the changes of the Ir surface structure. The kinetics of the NO + CO reaction have been studied using Pd [20] and Rh [22] single-crystal surfaces. In these studies, the apparent activation energies for N_2 and CO_2 formation were found to be almost independent

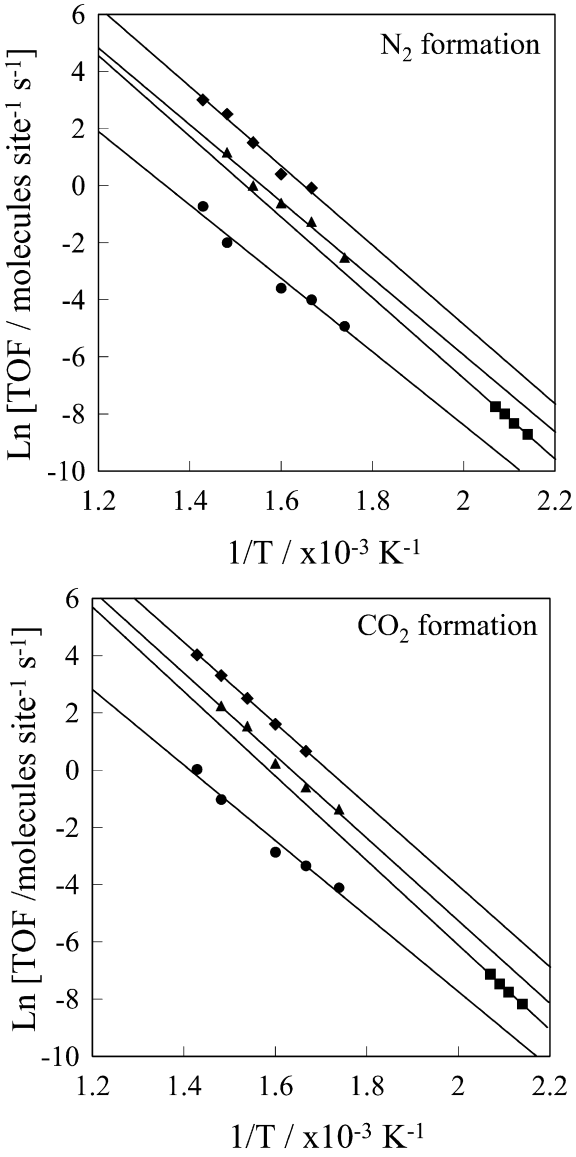

Fig. 6. Arrhenius plots of an Ir/SiO_2 powder catalyst (■), Ir(111) (●), Ir(211) (▲), and Ir(100) (◆) for N_2 and CO_2 formation from the NO + CO reaction. The powder catalyst data were obtained in the flow mode ($P_{NO} = P_{CO} = 5$ Torr in a He carrier gas), and the single-crystal data were acquired in the batch mode ($P_{NO} = P_{CO} = 5$ Torr).

of the surface structure, whereas the pre-exponential factor was strongly dependent on the surface structure. In our study, the pre-exponential factor was dependent on the Ir surface structure. Furthermore, the order of the pre-exponential factors for the various surface structures was in good agreement with the order of the planes with respect to NO dissociation activity. Goodman et al. [20] reported that removal of an inactive atomic nitrogen species may be important in determining the activity for N_2 and CO_2 formation over Pd surfaces. However, we found that the catalytic activity for NO reduction over Ir surfaces was dependent on the NO dissociation activity.

The activation energies for N_2 and CO_2 formation over an Ir/SiO_2 catalyst were estimated to be 117.2 ± 4.1 and 123.1 ± 4.1 kJ/mol, respectively, and these values were similar to those of the Ir single crystal. This result indicates that the NO + CO reaction proceeds on the Ir metallic surface over an Ir/SiO_2 powder catalyst. The TOFs for N_2 and CO_2 formation over Ir/SiO_2 were almost same for those for Ir(211), which indicates that the Ir surface structure of Ir/SiO_2 was close to that of Ir(211). That is, the Ir(211) surface can be regarded as an appropriate model catalyst for the NO + CO reaction over an Ir/SiO_2 catalyst because the apparent activation energies and the TOFs for N_2 and CO_2 formation over Ir(211) were in good agreement with those over the Ir/SiO_2 catalyst. It is generally considered that most of the N_2 is produced via NO dissociation and subsequent combination of N_a. If the N_2 is produced from this mechanism on the Ir surfaces, the reaction temperature for N_2 formation is dependent on the Ir surface structure because the N_2 desorption temperature on Ir(100) is 200 K lower than those on Ir(211) and Ir(111). However, N_2 formation activities were observed at the same reaction temperature region for all the Ir surfaces, suggesting that the N_2 was not formed by the recombination of N_a during NO + CO reaction.

Table 1
Apparent activation energies and pre-exponential factors for N_2 and CO_2 formation

Catalyst	E_a (kJ/mol)		υ (s^{-1})	
	N_2 formation	CO_2 formation	N_2 formation	CO_2 formation
Ir/SiO_2[a]	117.2 ± 4.1	123.1 ± 4.1	$10^{9.3\pm0.6}$	$10^{10.2\pm0.6}$
Ir(111)[b]	107.0 ± 10.6	109.6 ± 9.6	$10^{7.5\pm1.7}$	$10^{8.1\pm1.5}$
Ir(100)[b]	115.3 ± 9.5	117.8 ± 8.0	$10^{9.9\pm1.5}$	$10^{10.5\pm1.3}$
Ir(211)[b]	111.7 ± 8.7	120.3 ± 8.6	$10^{9.1\pm1.4}$	$10^{10.3\pm1.3}$

[a] Flow reaction at $P_{NO} = P_{CO} = 5$ Torr in a He carrier gas.
[b] Batch reaction at $P_{NO} = P_{CO} = 5$ Torr.

To clarify the details of the reaction mechanism, we measured surface adsorbates on Ir(211) under real reaction conditions using in situ PM-IRAS. We observed isocyanate (NCO) species at 2268 cm^{-1} [21,41–45] in addition to adsorbed CO species at reaction temperatures above 400 K (Fig. 7). The peak intensity of NCO was decreased at 600 K, which clearly indicates that NCO formation depended on the reaction temperature. Solymosi et al. reported the IR band of NCO species on metal and metal oxide surface, and they found that the preadsorbed oxygen atoms significantly stabilize the NCO species on Rh(111) [44,45]. In Fig. 8, the peak intensity for NCO species and the TOFs for N_2 formation over Ir(211) are plotted as a function of reaction temperature. The peak intensity for NCO species increased with increasing the reaction temperature and reached a maximum value at 600 K. Above 600 K, the peak intensity for NCO species greatly decreased with reaction temperature. In contrast, N_2 formation activity appeared above 600 K and greatly increased with increasing reaction temperature. The NCO species is an intermediate for NO reduction with hydrocarbons, and this intermediate reacts with NO to form N_2 and CO_2 on a Cu-ZSM-5 surface [41]. Surface isocyanates are intermediates for the NO + CO reaction, which react with NO to form gas-phase N_2O over a Rh surface [43]. On the other hand, Goodman et al. [21] reported that the isocyanate species plays the role of a spectator rather than an intermediate in CO + NO reaction over the Pd crystal because of the stability of the isocyanate species. However, the isocyanate species formed

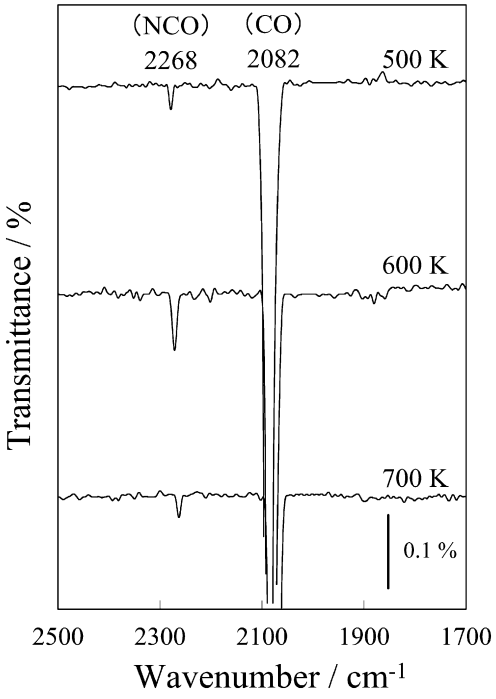

Fig. 7. In situ PM-IRA spectra of Ir(211) during exposure to a NO/CO (= 1) gas mixture at 10 Torr.

on the Ir surfaces is not so much stable under the reaction temperature region from the result of Fig. 8. Furthermore, Jentys et al. also reported [46] that the surface concentration of the isocyanate species was strongly correlated to the activity of the Pt/MCM-41 catalyst, whose relationship is in good agreement with the result of Fig. 8. They concluded that the isocyanate species was a reaction intermediate during the NO reduction. We thus believe that the NCO species is a reaction intermediate in our system and that the NO + CO reaction consists of the following elementary steps:

$$NO_a \rightarrow N_a + O_a, \quad (1)$$

$$N_a + CO_a \rightarrow NCO_a, \quad (2)$$

$$NCO_a + NO_a \rightarrow N_{2g} + CO_{2g}, \quad (3)$$

$$O_a + CO_a \rightarrow CO_{2g}. \quad (4)$$

We measured kinetic data for steps (1)–(4). First, we measured the NO dissociation kinetic data on the Ir surfaces. The dissociation kinetics of NO were measured at a constant temperature between 255 and 310 K in a vacuum. The initial NO coverage on the Ir surfaces was 0.25. Atomic nitrogen and oxygen were the only products formed by the dissociation of NO, and the formation ratio of O_a and N_a was almost 1. We measured the N_a coverage using XPS in isothermal decomposition experiments, and the rate constant was obtained from the slope of a plot of log Θ_{Na} versus t. Table 2 summarizes the kinetic data on the Ir surfaces. The activation energy was estimated to be 36 kJ/mol for all the Ir surfaces, and the pre-exponential factor and the reaction rates were strongly dependent on the surface structures, which indicated that the NO dissociation reaction was structure sensitive. The NO dissociation activity of the Ir planes decreased in the order (100) > (211) ≫ (111).

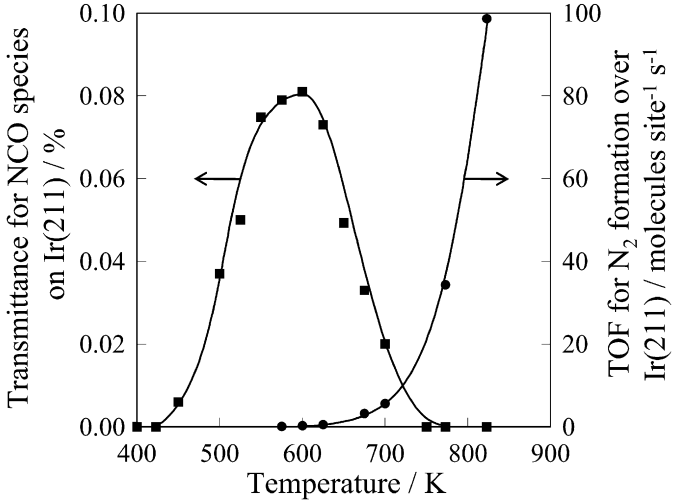

Fig. 8. Temperature dependence of NCO peak intensity (■) and TOF for N_2 formation (●) over Ir(211) during exposure to a NO/CO (= 1) gas mixture at 10 Torr.

Table 2
Apparent activation energies and pre-exponential factors for NO dissociation[a]

Catalyst	E_a (kJ/mol)	υ (s^{-1})
Ir(111)	36.6 ± 1.9	$10^{2.5\pm0.3}$
Ir(100)	36.0 ± 3.8	$10^{4.2\pm0.6}$
Ir(211)	35.4 ± 0.7	$10^{3.5\pm0.1}$

[a] The kinetic data were obtained at a constant temperature between 255 and 310 K in a vacuum. The initial NO coverage on the Ir surfaces was 0.25.

Table 3
Apparent activation energies and pre-exponential factors for NCO formation[a]

Catalyst	E_a (kJ/mol)	υ (s^{-1})
Ir(111)	43.8 ± 2.5	$10^{3.6\pm0.4}$
Ir(100)	42.6 ± 1.6	$10^{3.4\pm0.5}$
Ir(211)	41.2 ± 2.9	$10^{3.1\pm0.2}$

[a] The initial N_a coverage was 0.25. The Ir surfaces were exposed to 5 Torr of CO at a constant temperature between 325 and 350 K.

We thus considered the adsorbed NO species, both bridge NO and atop NO, were effectively dissociated on the Ir(100) surface. This order was in good agreement with that for the TOFs for NO reduction catalytic activity, which suggests that NO dissociation activity determined the total rate for the NO + CO reaction.

Next, we measured the formation rate of NCO using IRAS. First, we prepared atomic nitrogen by the dissociation of NO at 325–450 K. The initial N_a coverage was 0.25. Then the Ir surfaces were exposed to 5 Torr of CO at a constant temperature between 325 and 350 K. We measured the intensity of NCO species using IRAS, and we obtained the initial formation rates of NCO species from the slope of a plot of I_{NCO} versus t at zero coverage. The kinetic data are shown in Table 3. The activation energy and pre-exponential factor were determined to be 41–44 kJ/mol and $10^{3.1}$–$10^{3.6}$ s^{-1}, respectively. Values for all the surfaces were in good agreement with one another. Thus, we believe that the formation of NCO intermediates was independent of the Ir surface structures.

Table 4
Apparent activation energies and pre-exponential factors for NCO consumption[a]

Catalyst	E_a (kJ/mol)	υ (s^{-1})
Ir(111)	75.4 ± 2.3	$10^{8.5\pm0.4}$
Ir(100)	69.8 ± 2.8	$10^{7.9\pm0.5}$
Ir(211)	70.6 ± 1.0	$10^{8.0\pm0.2}$

[a] The Ir surfaces were exposed to 1×10^{-7} Torr of NO at a constant temperature between 300 and 325 K.

Finally, we measured the rate of NCO consumption. We confirmed that the NCO species did not decompose at temperatures below 333 K. However, we did observe a decrease in NCO coverage with exposure to NO on the Ir surface at temperatures between 300 and 325 K, which indicates that elementary step 3 proceeded on the Ir surfaces. We thus measured the intensity of NCO species with NO exposure at a constant temperature and determined the rate constant from the slope of a plot of $\log I_{NCO}$ versus t. The NO exposure pressure was 1×10^{-7} Torr. The apparent activation energy and pre-exponential factor for Ir(100) were determined to be 69.8 ± 2.8 kJ/mol and $10^{7.9\pm0.5}$ s^{-1}, respectively, and these values are in good agreement with those obtained for Ir(211) (70.6 ± 1.0 kJ/mol and $10^{8.0\pm0.2}$ s^{-1}) (Table 4). The apparent activation energy for Ir(111) (75.4 ± 2.3 kJ/mol) was slightly higher than the values for (100) and (211). In contrast, the NCO consumption rate on Ir(111) was slower than the rates on (100) and (211). Because the NO dissociation reaction was included in this elementary step, the reaction rate for NCO consumption was dependent on the Ir surface structure. We thus have elucidated the detailed kinetics and mechanism of the NO + CO reaction on Ir-based catalysts using surface-science techniques.

4. Conclusions

(1) NO adsorbed on the atop and hollow sites of Ir(111). On Ir(100), NO adsorbed on atop and bridge sites. NO adsorbed on the atop site of the (111) terrace and the bridge site of the (100) step over Ir(211). Only hollow NO desorbed to N_2 at 471 K and 574 K on Ir(111). Both atop NO and bridge NO almost completely desorbed to N_2 at 400 and 600 K on Ir(100) and Ir(211), respectively. The NO dissociation activity of the Ir planes decreased in the order (100) > (211) ≫ (111). The NO adsorption and dissociation activities were strongly dependent on the Ir surface structure.

(2) CO adsorbed only on the atop site over the Ir surfaces at 223 K, indicating that CO adsorption was independent of the Ir surface structures. On Ir(211), CO adsorbed initially on the (100) step and then began to adsorb on the (111) terrace after the step sites were saturated. The thermal stability of the adsorbed CO on Ir(100) was higher than that on Ir(111).

(3) Compared to Ir(100) and Ir(211), Ir(111) showed low activity for N_2 and CO_2 production from the NO + CO reaction. The TOFs for N_2 and CO_2 formation for the Ir planes decreased in the order (100) ⩾ (211) ≫ (111). This order was in good agreement with the order for NO dissociation activity, which indicates that the NO-reduction catalytic activity was dependent on the NO dissociation.

(4) The TOFs for N_2 and CO_2 formation from the NO + CO reaction over Ir/SiO_2 were almost same for those over Ir(211), which indicates that the Ir surface structure of Ir/SiO_2 was similar to the surface structure of Ir(211). Thus, we believe that the active site for the NO + CO reaction over Ir/SiO_2 was a metallic Ir surface.

(5) An NCO species was an intermediate for NO reduction with CO, and the NCO species reacted with NO to form N_2 and CO_2. From the kinetic study of the elementary steps, we concluded that the rate-limiting step for NO reduction with CO was the NO dissociation step. That is, the NO dissociation activity determined the total reaction rate.

Acknowledgment

This work was supported by the Japan Society for the Promotion of Science (JSPS-KAKENHI 17350079).

References

[1] V.I. Pârvulescu, P. Grange, B. Delmon, Catal. Today 46 (1998) 233.
[2] H. Hamada, Catal. Today 22 (1994) 21.
[3] R. Burch, J.P. Breen, F.C. Meunier, Appl. Catal. B 39 (2002) 283.
[4] M. Ogura, A. Kawamura, M. Matsukata, E. Kikuchi, Chem. Lett. (2000) 146.
[5] A. Wang, L. Ma, Y. Cong, T. Zhang, D. Liang, Appl. Catal. B 40 (2003) 319.
[6] M. Haneda, Pusparatu, Y. Kintaichi, I. Nakamura, M. Sasaki, T. Fujitani, H. Hamada, J. Catal. 229 (2005) 197.
[7] M. Shimokawabe, N. Umeda, Chem. Lett. 33 (2004) 534.
[8] A. Takahashi, I. Nakamura, M. Haneda, T. Fujitani, H. Hamada, Catal. Lett. 112 (2006) 133.
[9] H.S. Oh, C.C. Eickel, J. Catal. 128 (1991) 526.
[10] H.S. Oh, B.G. Fisher, E.J. Carpenter, W.D. Goodman, J. Catal. 100 (1986) 360.
[11] K.B. Cho, J. Catal. 148 (1994) 697.
[12] F. Schuth, E. Wicke, J. Phys. Chem. 144 (1985) 239.
[13] Y.K. Ng, N.D. Belton, J.S. Schmieg, B.G. Fisher, J. Catal. 146 (1994) 394.
[14] W.D. Goodman, Surf. Sci. 299/300 (1994) 837.
[15] W.D. Goodman, Chem. Rev. 95 (1995) 523.
[16] M.J.P. Hopstaken, W.J.H. van Gennip, J.W. Niemantsverdriet, Surf. Sci. 433–435 (1999) 69.
[17] T.W. Root, L.D. Schmidt, Surf. Sci. 150 (1985) 173.
[18] L.M. Carballo, T. Hahn, H.-G. Lintz, Appl. Surf. Sci. 40 (1989) 53.
[19] T. Hahn, H.-G. Lintz, Appl. Surf. Sci. 40 (1989) 59.
[20] D.R. Rainer, S.M. Vesecky, M. Koranne, W.S. Oh, D.W. Goodman, J. Catal. 167 (1997) 234.
[21] C. Hess, E. Ozensoy, D.W. Goodman, J. Phys. Chem. B 107 (2003) 2759.
[22] C.H.F. Peden, D.N. Belton, S.J. Schmieg, J. Catal. 155 (1995) 204.
[23] T. Fujitani, I. Nakamura, Y. Kobayashi, A. Takahashi, M. Haneda, H. Hamada, J. Phys. Chem. B 109 (2005) 17603.
[24] I. Nakamura, K. Suzuki, A. Takahashi, M. Haneda, H. Hamada, T. Fujitani, J. Vac. Sci. Technol. A 25 (2007) 1143.
[25] Ts. Marinova, L.K. Kostov, Surf. Sci. 185 (1987) 203.
[26] J.E. Muilenberg (Ed.), Handbook of X-Ray Photoelectron Spectroscopy, Perkin-Elmer, Eden Prairie, MN, 1979.
[27] J.S. Villarrubia, W. Ho, J. Chem. Phys. 87 (1987) 750.
[28] D.Y. Zemlyanov, M.Y. Smirnov, V.V. Gorodetskii, J.H. Block, Surf. Sci. 329 (1995) 61.
[29] C. Nyberg, P. Uvdal, Surf. Sci. 204 (1988) 517.

[30] A. Sandell, A. Nilsson, N. Mårtensson, Surf. Sci. 251/252 (1991) 971.
[31] J.F. Zhu, M. Kinne, T. Fuhrmann, R. Denecke, H.-P. Steinrück, Surf. Sci. 529 (2003) 384.
[32] I. Nakamura, T. Fujitani, H. Hamada, Surf. Sci. 514 (2002) 409.
[33] D. Ramsier, Q. Gao, H.N. Waltenburg, J.T. Yate Jr., J. Chem. Phys. 100 (1994) 6837.
[34] R.J. Behm, K. Christman, G. Ertl, J. Chem. Phys. 73 (1980) 2984.
[35] S. Surnev, M. Sock, M.G. Ramsey, F.P. Netzer, M. Wiklund, M. Borg, J.N. Andersen, Surf. Sci. 470 (2000) 171.
[36] H. Steinger, S. Lehwald, H. Ibach, Surf. Sci. 123 (1982) 264.
[37] R. Martin, P. Gardner, A.M. Bradshaw, Surf. Sci. 342 (1995) 69.
[38] A. Beutler, E. Lundgren, R. Nyholm, J.N. Andersen, B.J. Setlik, D. Heskett, Surf. Sci. 396 (1998) 117.
[39] F. Strisland, A. Ramstad, T. Ramsvik, A. Borg, Surf. Sci. 415 (1998) L1020.
[40] H. Orita, in preparation.
[41] H. Oka, T. Okada, K. Hori, J. Mol. Catal. 109 (1996) 51.
[42] H. Celio, K. Mudalige, P. Mills, M. Trenary, Surf. Sci. 394 (1997) L168.
[43] D.I. Kondarides, T. Chafik, X.E. Verykios, J. Catal. 193 (2000) 303.
[44] J. Kiss, F. Solymosi, J. Catal. 179 (1998) 277.
[45] F. Solymosi, T. Bánsági, J. Catal. 202 (2001) 205.
[46] W. Schießer, H. Vinek, A. Jentys, Appl. Catal. B 33 (2001) 263.